https://doi.org/10.1016/j.ijheatmasstransfer.2017.11.129

Oblique impact of two successive droplets on a flat surface

Shakeel Ahmad, Hui Tang*, Haimin Yao

Department of Mechanical Engineering, The Hong Kong Polytechnic University, Kowloon, Hong Kong SAR, China

*Corresponding author. Email: h.tang@polyu.edu.hk

Abstract

Using the lattice Boltzmann method, a numerical study was conducted to investigate the oblique impact of two successive droplets on a flat surface. The focus was placed on the effects of surface inclination, lateral/longitudinal offset, the impact dynamics of the two droplets and the subsequent dynamics of the combined droplet. The evolution of the topology, contact lines and spread factor of the two droplets under various conditions was compared and analyzed. It was found that, compared to single droplet impact, the impact of successive droplets shows quite different dynamics due to the involved coalescence process. The surface inclination causes asymmetric spreading of the droplets. The increase in surface inclination leads to faster downward spreading and reduced lateral spreading. The non-zero offset between the two droplets further enhances this asymmetry. Furthermore, the intermixing between the two droplets during the oblique impact was also examined. It was observed that the surface inclination changes the mass distribution of the combined droplet.

Keywords: Successive droplets; Oblique impact; Lateral/longitudinal offset; Lattice Boltzmann method.

1. Introduction

Impact of droplets on solid surfaces is a commonly observed phenomenon both in nature and in industrial applications, such as ink-jet printing [1, 2], plasma spraying, spray cooling [3], droplet fuel mixtures in internal combustion engines and microfluidics [4], and hence it is of fundamental and practical importance. In the past century the dynamics of droplet normally impacting on surfaces has been extensively investigated [5–13], which has been well reviewed by Yarin [14]. Apart from normal impact, works are also available in which oblique impact of single droplet is studied. Šikalo et al. [15] investigated droplet impact and spreading on dry walls and liquid films with low impact angles by looking at the effects of impact angle, Weber number and surface properties on the occurrence of droplet rebound. Lunkad et al. [16] studied the effects of surface inclination, surface properties, liquid properties and impact velocity on the dynamics in different regimes of droplet spreading: spreading and sliding, splash, and rebound and deformation. Particularly, they focused on surface wetting characteristics by using the static contact angle (SCA) and dynamic contact angle (DCA) models. They found that the DCA model performed better in predicting the spreading behavior. Shen et al. [17] used the lattice Boltzmann method (LBM) to study complex asymmetric spreading on slanted surfaces by investigating droplet spreading, contact line motion and topological evolution.

Impact of successive droplets further encompasses the dynamics of collision and coalescence of one droplet with another that is stationary or has hit the surface slightly earlier. The coalescence of a moving droplet with a stationary droplet on a surface has been studied both experimentally and numerically [18–20]. Li et al. [18] focused on the spread length and identified three different coalescence mechanisms. Graham et al. [19] carried out a combined experimental and numerical study on coalescence of two droplets with various wettability and offsets. It was found that the maximum spread length decreased with increasing the hydrophobicity and offset, but increased with the droplet inertia. The dynamics and intermixing of two similar-sized droplets normally impacting on a flat surface was studied by Castrejón-Pita et al. [20]. They did not see the occurrence

of mixing during the impact and coalescence. Roisman et al. [21] experimentally and theoretically studied the velocity, thickness and height of the uprising liquid sheet formed from the impact of two droplets. Raman et al. [22] reported the formation of crown and central uprising jet during the impact and subsequent coalescence of two droplets simultaneously impinging on a liquid film. Air bubbles entrapment and segment detachment from the surface depending on the Bond number and Weber number for two droplets impacting on a dry surface was investigated by Wu et al.[23]. Zhou et al. [24] applied an improved lattice Boltzmann method to investigate multiple droplet impact and subsequent interactions. Fujimoto et al. [25] also experimentally investigated the normal impact of two successive droplets, and looked at the influence of impact interval between the droplets on the evolution of the diameter of resulting liquid film. It was shown that, although the non-dimensional diameter of the liquid film is larger than that in the single droplet case, they share a similar variation trend. Tong et al. [26] observed two modes of interaction, namely in-phase and out-of-phase, depending on the interdroplet spacing. Their results indicated an increase in maximum spread factor with increasing trailing droplet velocity. Recently, Raman et al. [27] also studied the modes of droplet impact depending on the velocity ratio of the leading and trailing droplets. In addition, they investigated the droplet offset and observed asymmetric coalescence. By fixing the offset between two droplets, the same group [28] also studied simultaneous impact of the two droplets on a surface with one droplet having an oblique velocity, and observed the formation of asymmetric ridge.

Different from all the previous studies, in the present study we aim to investigate the dynamics of two successive droplets obliquely impacting on a flat surface, including both the impact process and the subsequent coalescence. The focus is placed on the effects of impact obliqueness (equivalently the surface inclination if the droplet velocity is fixed) and lateral/longitudinal offset between the two droplets. This study is directly motivated by fog harvesting, in which tiny fog droplets successively impinge on an inclined mesh, coalesce, grow in size, and roll off the mesh surface due to gravity [29]. Recently, bio-inspired meshes are being prepared for efficient fog collection. Such mesh wires can have a diameter (or width in case of flat ribbons) of micrometers [30], where the role of droplet

offset also becomes important for determining minimum mesh wire diameter (or ribbon width). This study is also important for the understanding of some natural phenomena, such as rain droplets impacting on car windscreen, spray coating where the droplet impact angle is a key for uniform deposition, and spray on plant leaves in agriculture herbicide applications [31].

The paper is organized as follows. In Section 2 the problem is defined and a dimensionless analysis is conducted. Section 3 introduces the numerical methodology with mesh specification and code validation. Section 4 presents the results and discussion on three selected parameters: surface inclination, lateral offset and longitudinal offset. Finally, conclusions are drawn from the present work.

2. Problem definition and dimensional analysis

Fig. 1 shows a schematic of the present problem. With the same velocities two identical droplets make successive impact on a slanted surface along the vertical direction. The two droplets are separated with a vertical distance and, in some cases, a lateral/longitudinal distance during the impact. To help facilitate the study, a Cartesian coordinate system is defined in such a way that its origin is located at the impact point of the leading droplet on the surface, and its x and y axes point to the lateral and longitudinal (slope) directions over the slanted surface, respectively.

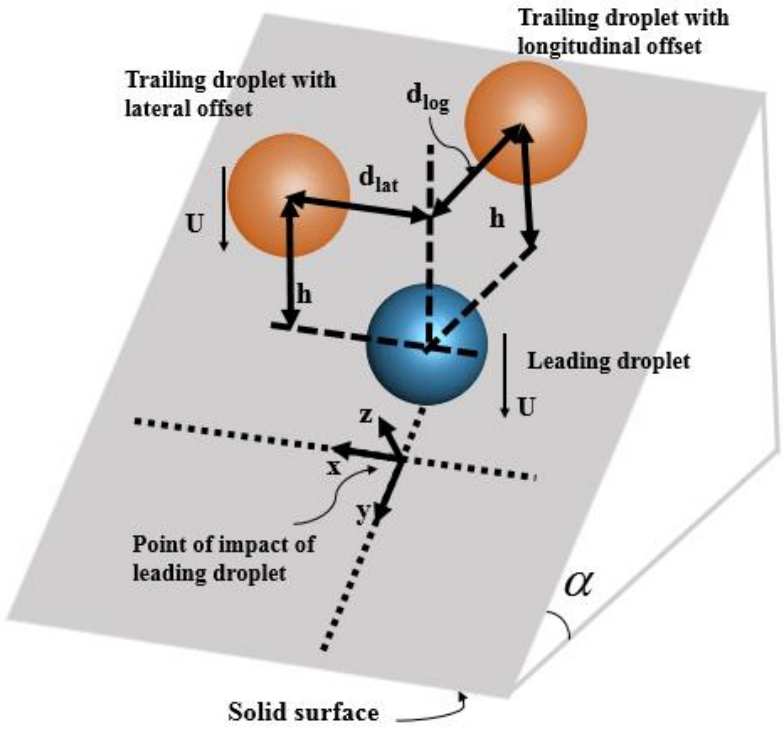

Fig. 1. Schematic of two successive droplets impacting on an inclined surface.

Assume there is no gravitational force. The dynamics of the two droplets are determined by twelve key parameters: the surface inclination angle α, the surrounding gas density ρ_g and viscosity μ_g, the liquid droplet diameter D, density ρ, viscosity μ, surface tension σ, contact angle θ and impact velocity U, and the center-to-center distance of the two droplets in the lateral direction d_{lat}, in the longitudinal direction d_{long}, and in the vertical direction h (see Fig. 1). According to the Buckingham-Pi theorem, these parameters can be condensed into following nine independent non-dimensional parameters:

$$\alpha,\ \rho/\rho_g,\ \mu/\mu_g,\ \mathrm{Re} = \rho UD/\mu,\ \mathrm{We} = \rho U^2 D/\sigma,\ \theta,\ \lambda_x = d_{lat}/D,\ \lambda_y = d_{long}/D,\ h/D \qquad (1)$$

where ρ/ρ_g and μ/μ_g are liquid-to-gas density ratio and viscosity ratio, respectively. The Reynolds number Re describes the relative importance of the fluid inertia compared to the viscosity force in the droplets, the Weber number We describes the relative importance of the fluid inertia compared to the surface tension of the droplets, and λ_x, λ_y and h/D describe the offsets between the two droplets along the x (lateral), y (longitudinal) and vertical directions, respectively. In literature the Ohnesorge number $\mathrm{Oh} = \mu/(\rho\sigma D)^{1/2}$ is also used to describe droplet dynamics [9,32], which can be related to Re and We

through Oh = $(We)^{1/2}/Re$.

In the present study, the properties of the two droplets and surrounding gas are fixed. That is, the density ratio ρ/ρ_g = 10.46, viscosity ratio μ/μ_g = 10.46, Reynolds number Re = 80, and Weber number We = 40 are all constants. In addition, among the three offsets of the two droplets, the vertical distance is fixed at h/D = 1.15. The contact angle of the droplets on the slanted surface is fixed at θ = 90°, a moderate value between hydrophobicity and hydrophilicity. Hence the focus is placed on the remaining three non-dimensional parameters, i.e., the inclination angle of the surface α, the lateral and longitudinal offsets between the two droplets λ_x and λ_y.

To describe the dynamics of the two successive impacting droplets, non-dimensional spread factors along the lateral and longitudinal directions are defined, respectively, as

$$S_x^* = S_x/D,\ S_y^* = S_y/D \tag{2}$$

where S_x and S_y are dimensional spread lengths defined as the largest distances of the contact edges of the two droplet system over the slanted surface in the x and y directions, respectively, as denoted in Fig. 2. In addition, a non-dimensional time t^* is used throughout this study to describe the temporal events

$$t^* = Ut/D \tag{3}$$

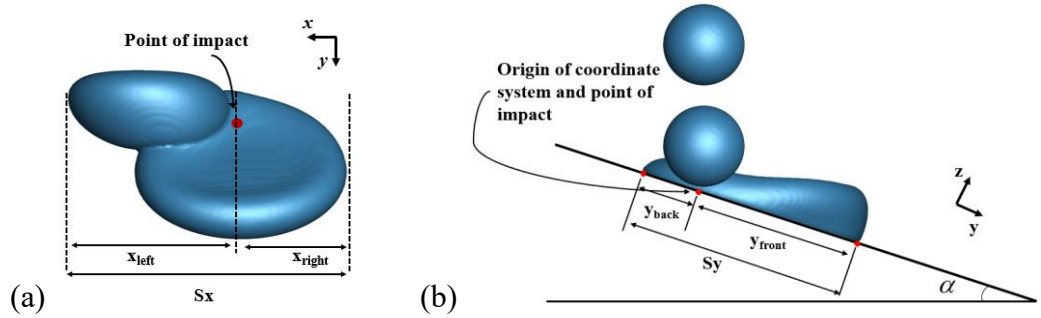

Fig. 2. (a) Lateral and (b) longitudinal spread lengths and motion of contact edges defined for the two droplet system.

3. Methodology

In this study, the lattice-Boltzmann method (LBM) was adopted to simulate the two-phase fluid flow since handling the liquid-gas interface using this method is relatively

easier [33]. The fundamentals of this method can be found in many review articles [33,34] and monographs [35,36], and hence are only briefly introduced here. In this study we used the LBM based on He et al.'s model [37]. In this method, two sets of distribution function, namely a pressure distribution function and a distribution function for index function, are used, and the phase segregation and interfacial dynamics are achieved by incorporating molecular interactions. The Navier-Stokes equation and interface-tracking equation can be recovered from the LBM equations of pressure distribution and index function, respectively [37,38]. The present LBM framework can achieve the second order accuracy in both space and time [38].

3.1 Computational domain and boundary conditions

The computational domain is a three-dimensional rectangular box. Its lower boundary is set as the slanted surface. The two droplets are placed inside the domain with preset offsets. Instead of redefining the surface, the change of impact obliqueness or surface inclination angle α is realized by relocating the two droplets such that the angle between the line connecting their centers and the surface's normal direction is equal to α. The periodic boundary condition is applied on the domain's four side boundaries, and the bounce back boundary condition is employed on the top and bottom boundaries to implement the no-slip boundary condition.

A grid dependence test has been conducted using four sets of grids as listed in Table 1. The maximum spread factors (S_x^* and S_y^*) for successive droplet impact on a surface of inclination 45° were calculated. It was found that relative errors in both the spread factors for a droplet having a diameter of 40 lattice units is less than 0.5% compared to that having a diameter of 60 lattice units. Therefore, by considering the trade-off between the accuracy and the computational cost, 40 lattice units per droplet diameter was chosen for the present study. During the simulations, the two droplets are firstly equilibrated for 15,000 time steps and are then allowed to move and impact on the slanted surface. The spurious current was found to be in the order of 10^{-5} lattice unit per time step, about three orders of magnitude less than the droplet impact velocity. Hence the effect of spurious current can be neglected.

As mentioned in Section 2, in this study the liquid-gas density ratio is fixed at only

ρ/ρ_g = 10.46. The use of this low density ratio is mainly determined by the limitation of the current LBM code. The simulation became unstable when the density ratio is higher than this value. However, since the Reynolds number and Weber number used in the present study are not high, so that the inertial effects in the surrounding gas are small, it is believed that the use of such a moderate density ratio is still able to capture the key dynamics of the two droplets successive impact problem.

Table 1. Grid independence test for droplet diameter at Re = 80 and We = 40

D (lattice units)	30	40	50	60
S_y^*(max)	2.446	2.469	2.473	2.479
Error	1.33%	0.40%	0.24%	-
S_x^*(max)	2.128	2.15	2.154	2.16
Error	1.48%	0.463%	0.27%	-

3.2 Validation

As an important benchmark for validation, the Laplace law relates the pressure difference across the droplet interface ΔP to the surface tension σ

$$\Delta P = \sigma/R \tag{4}$$

where R is the droplet radius. A droplet is initialized and equilibrated in a periodic domain of 120×120×120. Fig. 3 plots the pressure difference against the inverse of droplet radius, where a good agreement between the simulation and analytical results has been achieved.

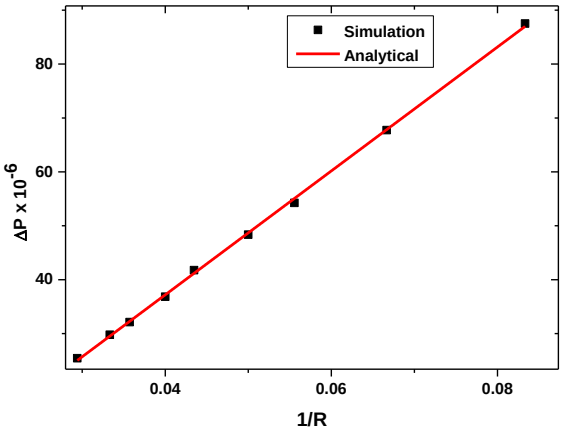

Fig. 3. Validation of the current LBM framework using the Laplace law for a stationary droplet.

To further validate the present simulation framework, the dynamic process of single

droplets normally impacting on a flat surface is simulated. Fig. 4 shows the typical evolution of the spread factor S^* of single, normally impacting droplets. This dynamic process generally consists of four consecutive phases, i.e., the kinematic phase, spreading phase, relaxation phase and equilibrium phase [5].

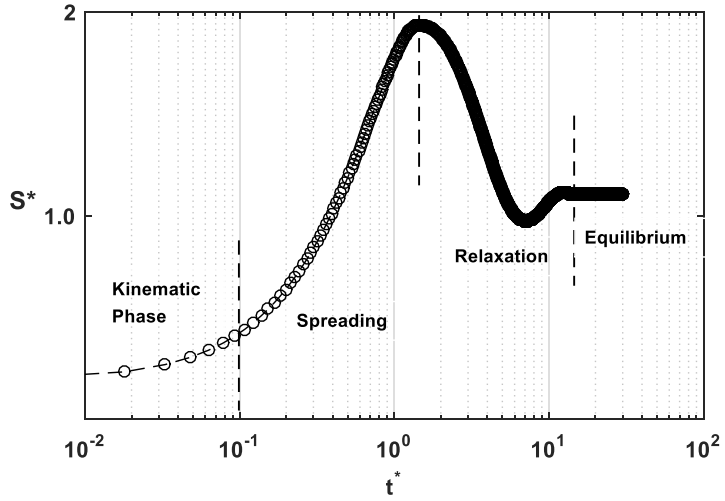

Fig. 4. Typical evolution of spread factor of a single droplet normally impacting on a flat surface.

The simulation results are firstly validated against existing experimental data. In the experiment [39], the normal impact of a droplet of diameter 2.45 mm was considered, which is a mixture of water and glycerin, with the density of 1,220 kg/m^3, surface tension of 0.063 N/m, and viscosity of 116 mPa·s. A wax surface, having contact angle hysteresis with advancing contact angle θ_a = 97° and receding contact angle θ_r = 90°, was used for the impact. Two cases with impact velocities of 1.04 m/s and 1.41 m/s were conducted, corresponding to Re = 27, We = 51 and Re = 36, We = 93, respectively. Simulations are performed accordingly, in which the contact angle hysteresis is modeled by following Wang et al. [40]. The spread factor is obtained for the kinematic phase, the spreading phase and a part of the relaxation phase, as shown in Fig. 5. It can be seen that reasonable agreement between the experimental data and the simulation results is achieved.

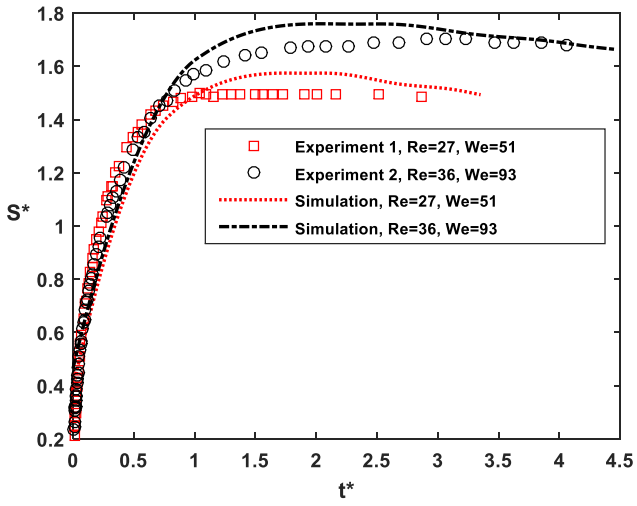

Fig. 5. Evolution of spread factor of single, normal impacting droplets in kinematic, spreading and part of relaxation phases.

Validation is then made by examining the droplet dynamics in the kinematic phase ($t^* << 1$) and the maximum spread factor. In reference [5], it was reported that the spread factor is proportional to $(t^*)^{1/2}$ in the kinematic phase with a coefficient of 2.8. Various numerical studies [7–9,41,42] were also carried out and obtained the coefficient varying from 1.35 to 2.5. Moreover, theoretical analysis predicted a value 2.0 for the coefficient [7, 12]. Using the present LBM framework, six cases are simulated at different Reynolds and Weber numbers. As shown in Fig. 6, a curve fitting gives $S^* = 1.9(t^*)^{1/2}$, where the coefficient value is close to the theoretically predicted value 2.0. Furthermore, the same set of data predicts that the maximum spread factor of single, normal impacting droplets has a good power law with $\mathrm{Re}^2\mathrm{Oh}$ as revealed in Fig. 7, which agrees well with what have been reported in literature [6,9,11] and also with a more specific relation obtained experimentally by Scheller et al. [32]

$$S^*_{\max} = 0.61\left(\mathrm{Re}^2\, Oh\right)^{0.166} \tag{5}$$

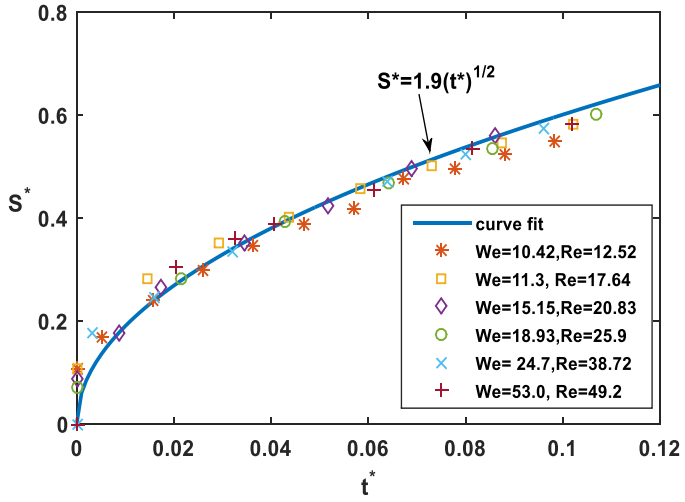

Fig. 6. Evolution of spread factor of single, normal impacting droplets in kinematic phase

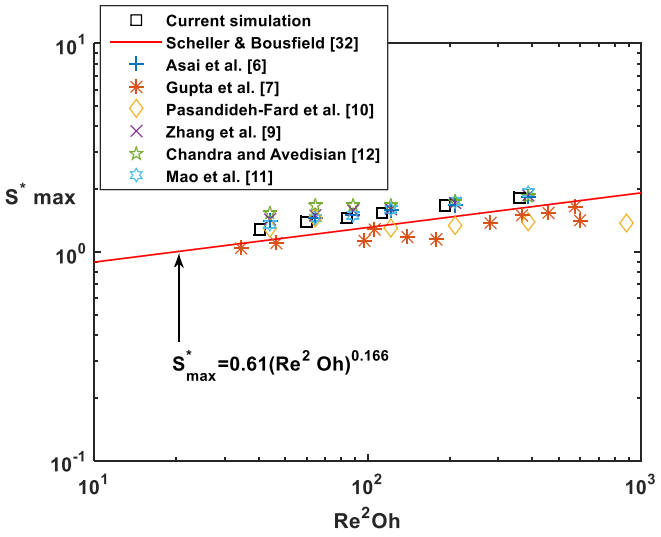

Fig. 7. Correlation of the maximum spread factor of single, normal impacting droplets with Re^2Oh

Finally, the validation is conducted on the impact and coalescence of two droplets, where the position of the second droplet can significantly affect the maximum spread factor. Graham et al. [19] investigated the impact of a falling droplet with a stationary droplet, and proposed empirical correlations for the maximum spread factor over different surfaces.

$$S^* = S / (D + d) \tag{6}$$

$$S^*_{max} = 1.322(1 + d/D)^{-0.9220}\,\mathrm{We}^{0.1943} \tag{7}$$

where d is the offset. Simulations are performed over a surface having contact angle hysteresis with an advancing contact angle $\theta_a = 108° \pm 5$ and a receding contact angle $\theta_r = 71° \pm 5$, and a static contact angle of $\theta = 93° \pm 3$. The dimensionless number are chosen

the same as in the single droplet validation cases, i.e., Re = 38.72 and We = 24.7. The simulated maximum spread factors are compared with those given by an empirical correlation Eq. (7) as listed in Table 2. The maximum error is found to be about 4%.

Table. 2. Maximum spread factor results for coalescence of two droplets at Re = 38.72 and We = 24.7

Offset ratio (d/D)	0	0.25	0.50	1.0
S^*_{max} (Eq. 7)	2.46	2.0	1.69	1.30
S^*_{max}(Simulation)	2.5	1.92	1.63	1.35
Error	1.66%	-4.0%	-3.5%	3.7%

4. Results and Discussion

4.1 Effect of two successive impacts

Figure 8 shows the evolution of the simulated two droplets successively impacting on a surface with an inclination angle of $\alpha = 45°$. The corresponding velocity fields inside and around the droplets in the mid-span plane are shown in Fig. 9. At an instant before the trailing droplet hits the surface (e.g., $t^* = 1.0$, shown in Fig. 8(a)), the leading droplet starts its spreading process. Instead of axisymmetric spreading in normal impact events, the presence of surface inclination results in different spreading along the two major directions, i.e., the lateral spreading along x direction and the longitudinal spreading along y direction. In addition, the centroid of the leading droplet moves downward along the inclined surface due to the relative fluid motion inside the droplet and the surface friction, as depicted in the velocity field in Fig. 9(a). At $t^* = 1.66$, the trailing droplet hits the spreading leading droplet which does not fully slide away, and the two droplets start coalescing. During the early stage of the coalescence (e.g., at $t^* = 3.0$ as shown in Fig. 8(b)), the two droplets merge and generate a combined, larger droplet, causing significant increase of both lateral and longitudinal spreading as compared to the spreading of each individual droplet (as quantified in Fig. 10). It is also seen from the velocity field shown in Fig. 9(c) that the trailing droplet injects high momentum fluid into the leading droplet through the coalescence, further enhancing the spreading. After the spreading in both directions reaches their respective maximum, the combined droplet starts its recoiling

process due to the surface tension, as revealed in Figs. 8(d) to 8(f), at $t^* = 6.0$, 9.0 and 13.0, respectively. In this recoiling process, the velocity near the front contact edge of the combined droplet becomes small and even reverses to form a vortex, while the velocity near the back contact edge is large, as revealed in Figs. 9(d) to 9(f). As such, the longitudinal spreading of the combined droplet reduces, and the height increases.

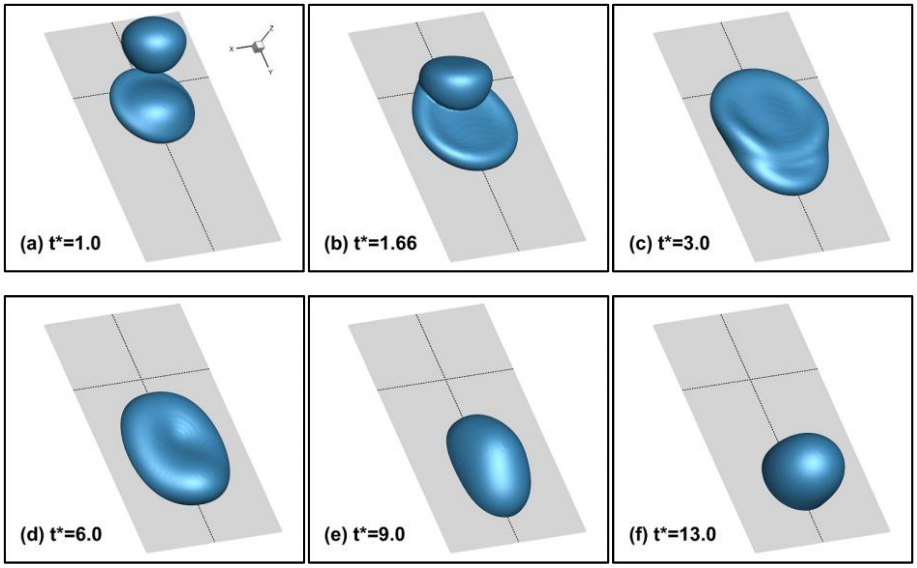

Fig. 8. Evolution of two droplets successively impacting on a surface with an inclination angle of $\alpha = 45°$. The intersection point of the two dashed lines on the surface indicates the point of impact for the leading droplet.

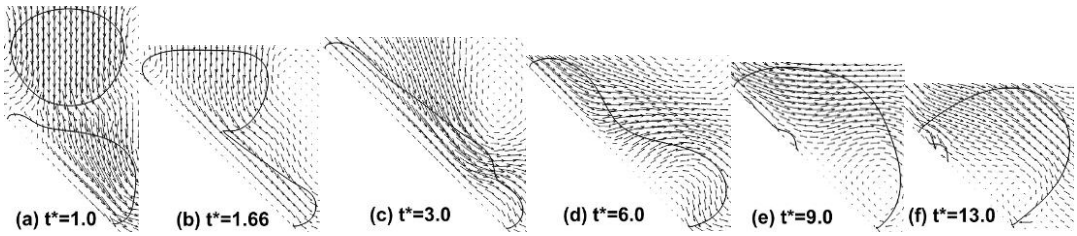

Fig. 9. Evolution of the velocity field inside and around the two droplets in the mid-span plane (i.e., the $x = 0$ plane).

Figure 10 further compares the evolution of spread factors of the two successively impacting droplets and of a single droplet. It is observed that, in the present case of two successively impacting droplets, the coalescence occurs when the leading droplet is in its spreading phase. After the coalescence, abrupt jumps in both the lateral and longitudinal spread factors occur, which, as having been explained above, is attributed to the injection of high momentum fluid from the trailing droplet. Note that the two spread factors reach their respective maximum at different timings. That is, the longitudinal spreading reaches

its maximum value first at about $t^* = 2.8$, which is very close to $t^* = 2.66$ for the single droplet, while the lateral spreading reaches its maximum at about $t^* = 3.92$, significantly delayed from $t^* = 2.01$ for the single droplet. It is also observed that a small plateau appears in the curve of two-droplet longitudinal spread factor during about $t^* = 5.0$ to 7.0, which defers the decrease of spread factor. Detailed inspection of Figs. 8 and 9 reveals that this plateau corresponds to the arrival of the trailing droplet front to the combined droplet front. Although the simulation time is not long enough to show the final trend, it is seen that, as time advances, both the spread factors of the two droplets gradually approach those for the single droplet.

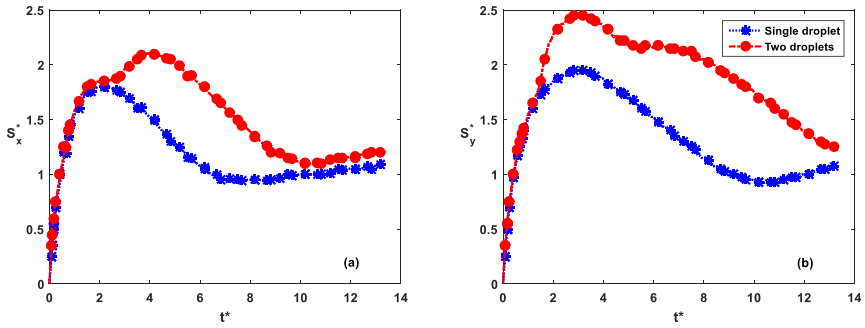

Fig. 10. Comparison of the evolution of (a) lateral and (b) longitudinal spread factors between a single impacting droplet and two successively impacting droplets.

4.2 Effect of surface inclination angle

The evolution of the two droplets successively impacting on surfaces with three different inclination angles, i.e., $\alpha = 30°$, 45° and 60°, is presented in Fig. 11. It is seen that with the increase of the inclination angle, the leading droplet slides faster, and hence the longitudinal distance between the two droplets increases when the trailing droplet hits the surface. As such, in the $\alpha = 30°$ and 45° cases the trailing droplet can still entirely fall on the leading droplet, but in the $\alpha = 60°$ case it only partially falls on the leading droplet. For this reason, the droplet dynamics in the $\alpha = 60°$ case is quite different from that in the other two cases, especially during the spreading and relaxation phases.

The evolution of laterally left/right contact edges and longitudinally front/back contact edges of the combined droplet for the three cases is compared in Fig. 12, and the evolution of their respective distances, i.e., the lateral and longitudinal spread factors, are

plotted in Fig. 13. It is seen from Fig. 12(a) that the left/right contact edges are symmetric about the mid-span plane (x = 0) in all the cases. During the spreading and relaxation phases (about $t^* < 10$), the distance between the left and right edges, i.e., the lateral spread factor, slightly decreases with the increase of the surface inclination angle, which is also confirmed in Fig. 13(a).

As for the motions of the front and back contact edges, as shown in Fig. 12(b), both edges move downward (along the positive y direction) faster with the increase of inclination angle, confirming the sliding trend observed in Fig. 11. The back contact edges in all the cases experience a short upward motion (along the negative y direction) before moving downward, which is the result of spreading. For the α = 60° case, an upward jump in the back contact edge is observed, starting at about t^* = 1.66. This is due to the partial contact of the trailing droplet with the already-on-surface leading droplet as revealed in Fig. 11(c1). This abrupt jump is also observed in the evolution of longitudinal spread factors in Fig. 13(b).

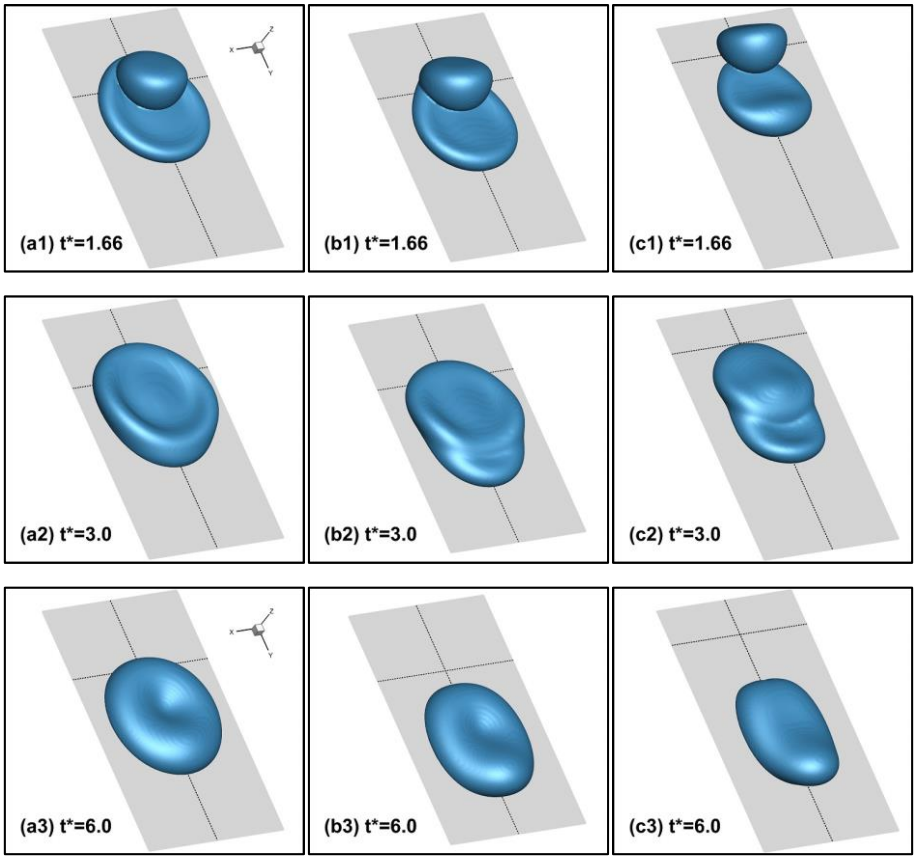

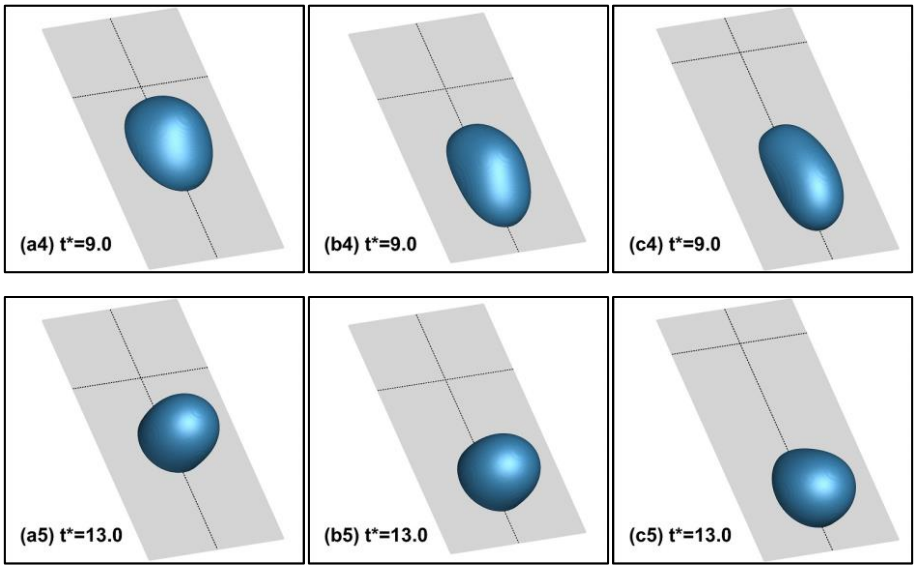

Fig. 11. Evolution of two droplets successively impacting on surfaces of different inclination angles: (a) α = 30°, (b) α = 45°, and (c) α = 60°. The intersection point of the two dashed lines on the surface indicates the point of impact for the leading droplet.

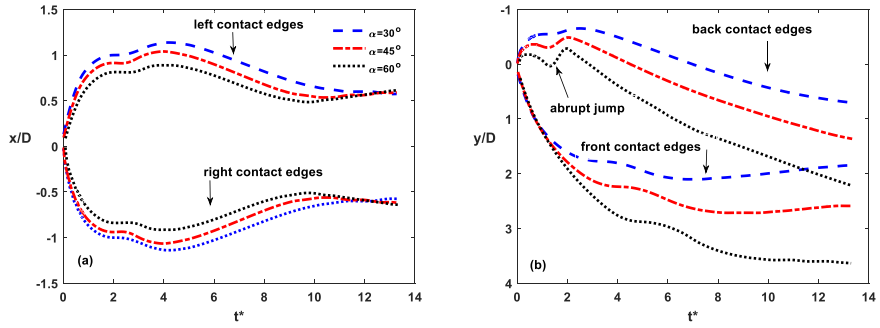

Fig. 12. Evolution of (a) left and right edges and (b) front and back edges of the combined droplet at different surface inclination angles.

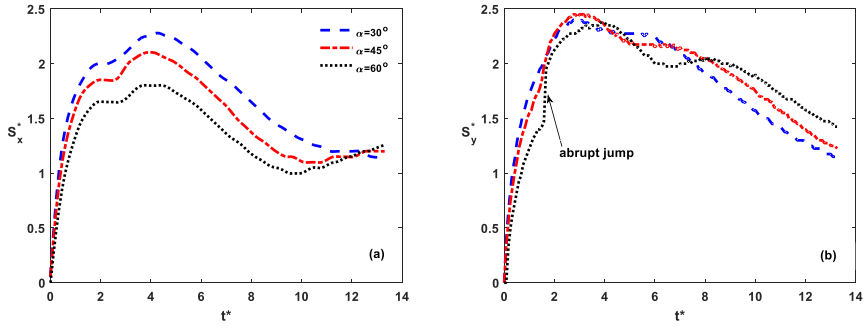

Fig. 13. Evolution of (a) lateral and (b) longitudinal spreading factors at different surface inclination angles.

4.3 Effect of lateral offset

The evolution of the two droplets successively impacting on a surface of an inclination angle $\alpha = 45°$ with various lateral offsets, i.e., $\lambda_x = 0.50$, 0.75, 1.0 and 1.5, is presented in

Fig. 14. It is seen that, due to the non-zero lateral offset, the coalescence of the two droplets in all the cases becomes asymmetric about the mid-span plane ($x = 0$). When the trailing droplet hits the surface, the overlap between the two droplets becomes smaller with the increase of lateral offset, and the subsequent coalescence process lasts for a longer time. Note that the two droplets will never merge if the lateral offset is greater than about 1.5. In the λ_x = 0.50, 0.75 and 1.0 cases, clear capillary wave propagation is observed during the coalescence process at t^* = 3.0. When this wave front reaches the front contact edge of the leading droplet at t^* = 6.0, a bulge appears at the front. At this instant, a slight corner shape is observed at the back contact edge of the combined droplet in the λ_x = 0.75 and 1.0 cases (see Figs. 14(b3) and 14(c3)), which is attributed to the intermediate lateral offset. As for the λ_x = 1.5 case, since the lateral offset is large, a combined droplet of dumbbell shape is observed at t^* = 6.0 as shown in Fig. 14(d3). After t^* = 6.0, the surface tension force dominates in all the cases and the droplet retraction begins. At t^* = 13.0, the combined droplets in the λ_x = 0.50, 0.75 and 1.0 cases share a similar shape, while the droplet in the λ_x = 1.5 case is elongated in the lateral direction.

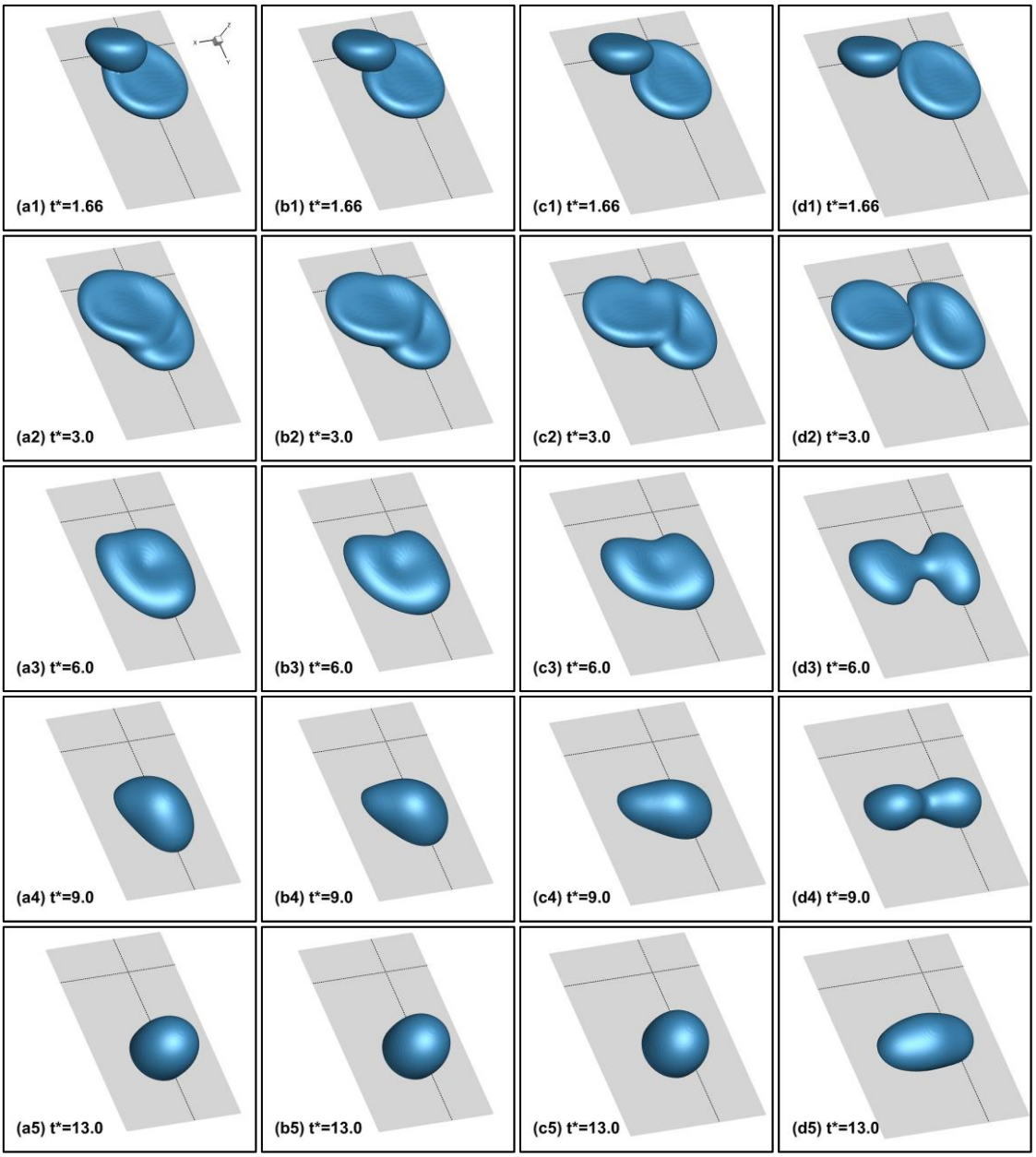

Fig. 14. Evolution of two droplets successively impacting on a surface of inclination α = 45° with various lateral offsets. From left to right: λ_x = 0.5, 0.75, 1.0 and 1.5. The intersection point of the two dashed lines on the surface indicates the point of impact for the leading droplet.

The evolution of the left/right and front/back contact edges of the combined droplets for these four cases is shown in Fig. 15. The data from the zero-offset case is also plotted as a reference. It can be seen from Fig. 15(a) that, with the increase of lateral offset, the abrupt increase of the left contact edge at about t^* = 1.66 becomes more obvious, and the subsequent peak gets higher. For the right contact edge, however, the introduction of non-zero lateral offset makes it slightly retreat. As a result, the lateral spread factor, i.e., the distance between the left and right contact edges, increases with the increase of lateral

offset, as revealed in Fig. 15(c).

As for the front contact edges, it is seen from Fig. 15(b) that in the beginning they all spread very similarly. Starting from $t^* = 4.5$, an abrupt change is observed, which is a clear sign of the arrival of high-momentum fluid from the trailing droplet. This sudden change is largest in the zero-offset case and decreases with the lateral offset. In the largest offset case where $\lambda_x = 1.5$, however, such a sudden change is not observed owing to the bare coalescence of the two droplets. This abrupt change also appears in the spreading of the back contact edge at around $t^* = 1.6$. After this instant, the back-edge spreading decreases with the increase of the offset. Due to the less interaction, this sudden change is not obvious for the largest two offset cases where $\lambda_x = 1.0$ and 1.5. Different from its lateral counterpart, the longitudinal spread factor decreases with the increase of lateral offset, as depicted in Fig. 15(d).

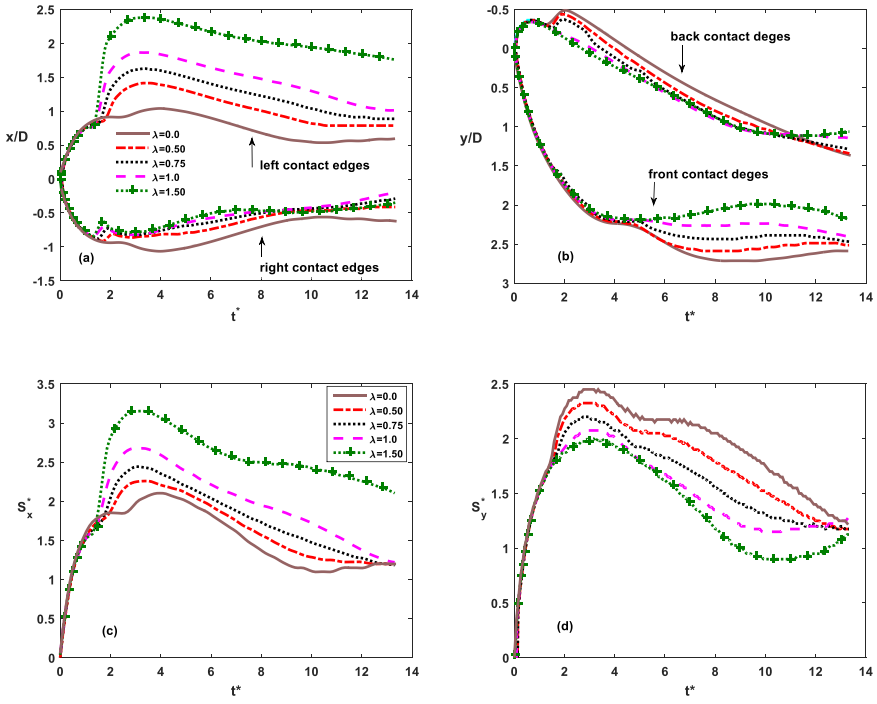

Fig. 15. Evolution of (a) left and right contact edges, (b) front and back contact edges, (c) lateral spread factor and (d) longitudinal spread factor of the combined droplet on a surface of inclination $\alpha = 45°$ with various lateral offsets.

4.3 Effect of longitudinal offset

The dynamics of the combined droplet also changes if the two droplets are offset in the longitudinal direction, i.e., in y direction. In the present study, three non-zero

longitudinal offsets are considered, i.e., λ_y = 0.25, 0.5 and 0.75. It was found that the two droplets do not merge if λ_y is greater than about 0.75.

The topological evolution of the two droplets with different longitudinal offsets is shown in Fig. 16. It is seen that, due to the offset, at t^* = 1.0 the trailing droplet partially hits the leading droplet in the λ_y = 0.25 and 0.5 cases, whereas it completely hits the dry surface in the λ_y = 0.75 case. Comparison of the coalescence process in these three cases reveals that the increase of longitudinal offset increases the longitudinal spreading of the combined droplet. This is also confirmed by the evolution of the droplet's front and back contact edges and the resulting longitudinal spread factor shown in Fig. 17. From Fig. 17(b), it is seen that the increase of longitudinal spreading is mainly attributed to the abrupt change of the back contact edge due to the landing of the trailing droplet. As for the evolution of the left and right contact edges of the combined droplet, it is seen from Fig. 17(a) that both edges are symmetric about the mid-span plane, and shift inwards with the increase of longitudinal offset. As such, the lateral spread factor reduces with the increase of the longitudinal offset as revealed in Fig. 17(c)

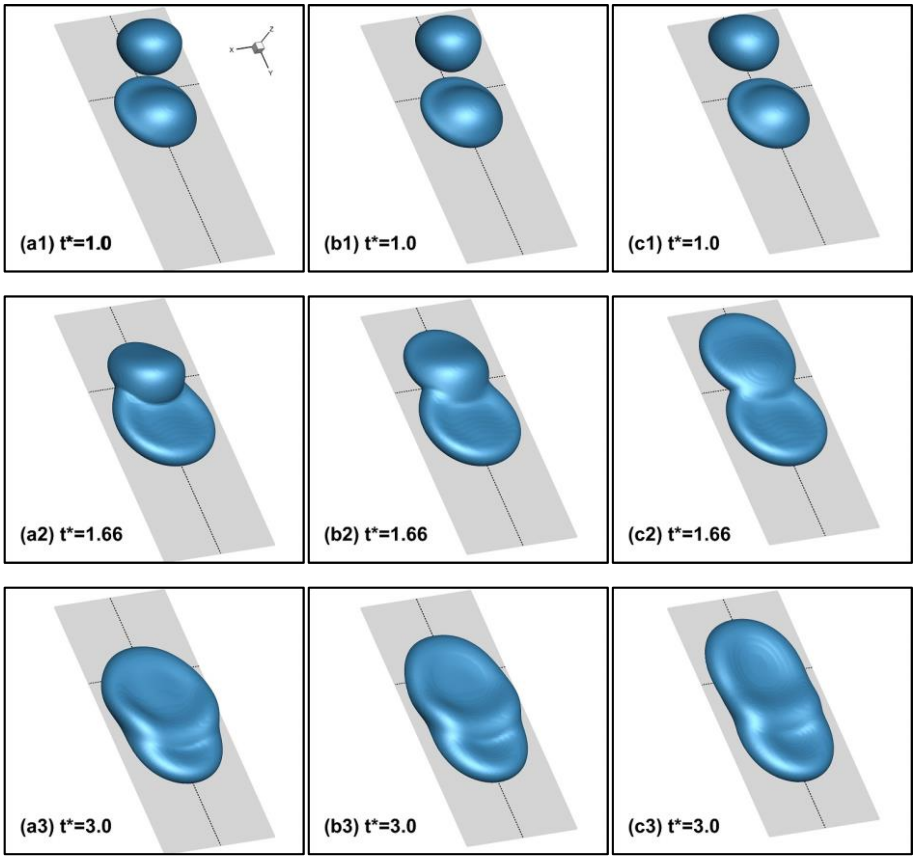

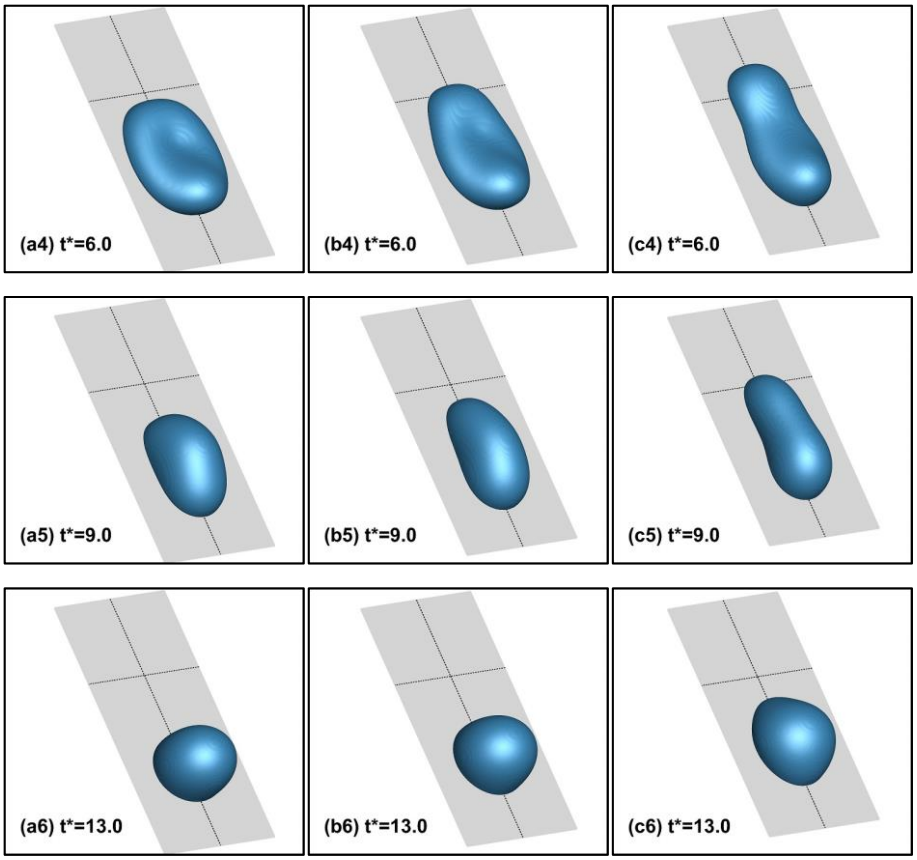

Fig. 16. Evolution of two droplets successively impacting on a surface of inclination α = 45° with various longitudinal offsets. From left to right: λ_y = 0.25, 0.5 and 0.75. The intersection point of the two dashed lines on the surface indicates the point of impact for the leading droplet.

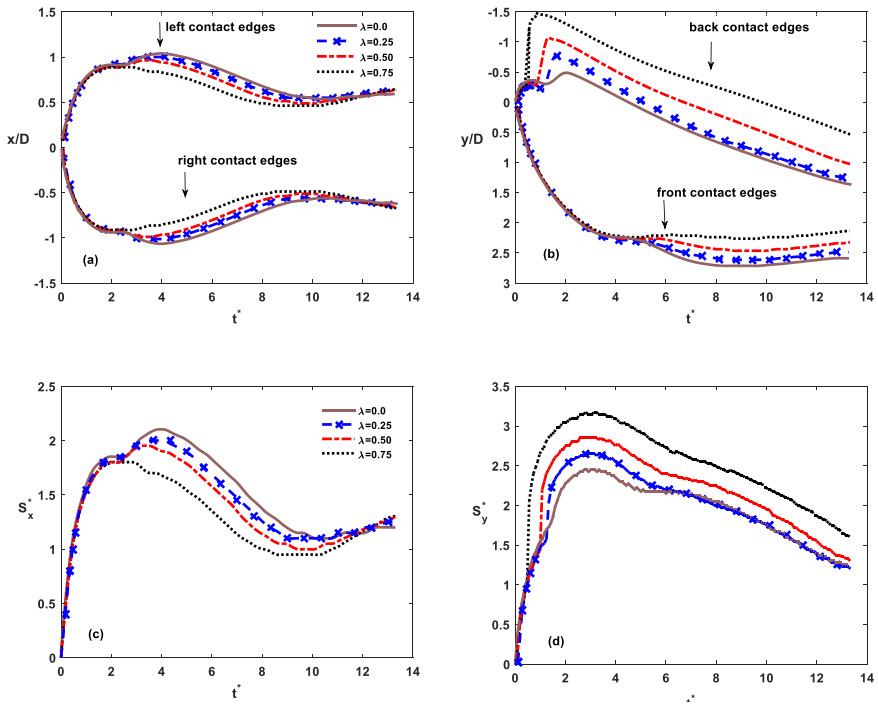

Fig. 17. Evolution of (a) left and right contact edges, (b) front and back contact edges, (c) lateral spread factor and (d) longitudinal spread factor of the combined droplet on a surface of inclination α = 45° with various longitudinal offsets.

4.4 Droplet intermixing

The intermixing of the two droplets during the impact and coalescence process is also investigated. To visualize the mixing process, tracer particles of two different colors are seeded inside the two droplets, whose trajectories are computed during the simulations. Fig. 18 shows the intermixing of the two zero-offset droplets successively impacting on surfaces of different slopes from two views, i.e., the mid-length view along the y axis as shown in the upper row and the mid-span view along the x axis as shown in the lower row. The leading droplet is filled with red tracer particles, whereas the trailing droplet is filled with green tracer particles. Evolution of the green particles clearly shows that upon collision the trailing droplet first penetrates the rear portion of the leading droplet, and then slides over the leading droplet to reach its front. With the increase of surface inclination angle, the green particles become less in the rear portion of the combined droplet and more in the front, indicating the change of mass distribution of the two droplets.

When the non-zero lateral offsets are introduced, the two droplets gradually become distinguishable in the lateral direction with a clear interface between them, as shown in the first row of Fig. 19. In the λ_x = 1.5 case where the lateral offset is the largest, this interface becomes vertical and coincides with the mid-span plane. Accordingly, the green particles observed from the mid-span become less and less, as shown in the lower row of Fig. 19. All these observations indicate that the intermixing is reduced with the increase of lateral offset.

When the non-zero longitudinal offsets are introduced, the trailing droplet is left further behind the leading droplet. Hence, with the increase of longitudinal offset, more green particles are accumulated in the rear portion of the combined droplet, and less are scattered in the front portion, as shown in Fig. 20, indicating the reduced intermixing.

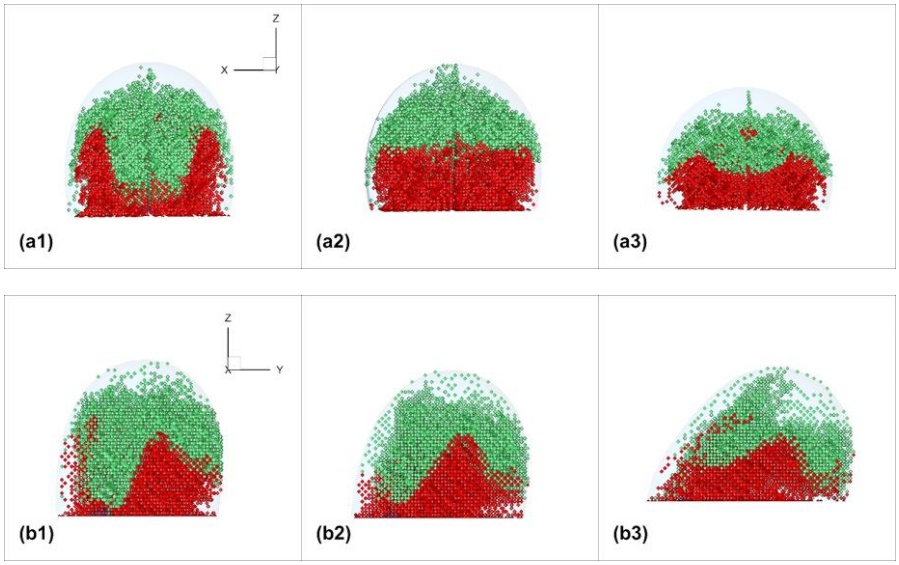

Fig. 18. Snapshots at $t^* = 13$ showing the intermixing of the two zero-offset droplets successively impacting on surfaces of different inclination angles. From left to right: $\alpha = 30°$, 45° and 60°; Top row: the mid-length view along the y axis; Bottom row: the mid-span view along the x axis.

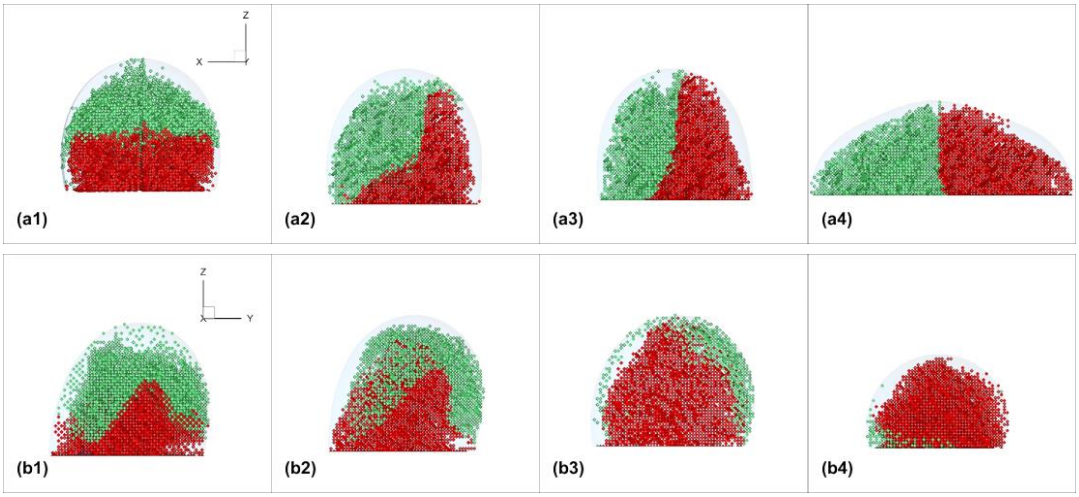

Fig. 19. Snapshots at $t^* = 13$ showing intermixing of the two droplets successively impacting on a surface of inclination $\alpha = 45°$ with various lateral offsets. From left to right: $\lambda_x = 0$, 0.5, 1.0 and 1.5; Top row: the mid-length view along the y axis; Bottom row: the mid-span view along the x axis.

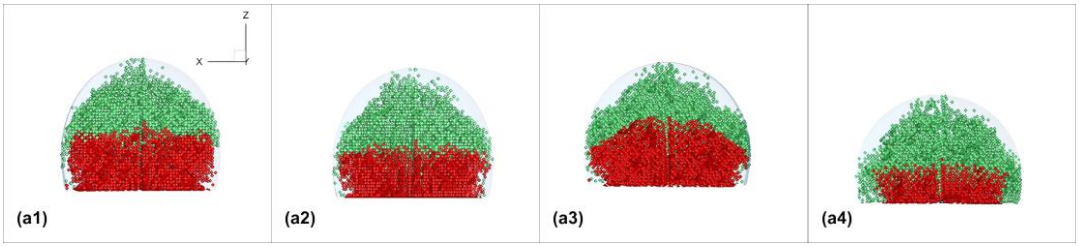

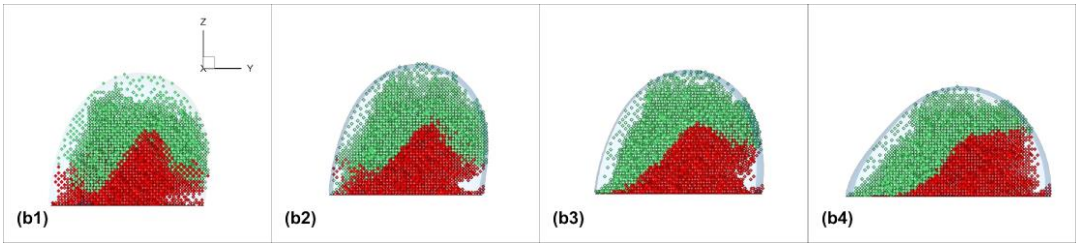

Fig. 20. Snapshots at $t^* = 13$ showing intermixing of the two droplets successively impacting on a surface of inclination $\alpha = 45°$ with various longitudinal offsets. From left to right: $\lambda_y = 0$, 0.25, 0.5 and 0.75; Top row: the mid-length view along the y axis; Bottom row: the mid-span view along the x axis.

5. Conclusion

In this study, the dynamics of two identical droplets successively and obliquely impacting on a flat surface has been investigated using three-dimensional LBM simulations. It was first demonstrated that the interaction between two successively impinging droplets can result in quite different dynamics compared to that of single droplets. The focus was then placed on the effects of impact obliqueness (or surface inclination) and the lateral/longitudinal offsets on the two droplets' impact and coalescence processes. The major findings are summarized as follows:

1) Oblique impact causes asymmetric droplet spreading, with the downward spreading dominant over the lateral spreading. The increase in the surface slope leads to faster downward spreading and reduced lateral spreading.
2) The coalescence of the two droplets can result in abrupt changes in the evolution of the back and left/right contact edges, which is attributed to the partial landing of the trailing droplet on the leading droplet.
3) The offset between the two droplets further increases the asymmetry of the combined droplet's dynamics. The increase of lateral offset causes the increase of the maximum lateral spread factor and the reduction of the maximum longitudinal spread factor, whereas the increase of longitudinal offset results in the opposite change.
4) The impact obliqueness or inclination of the surface changes the intermixing of the two droplets and hence the mass distribution of the combined droplet. In addition, the introduction of lateral or longitudinal offsets reduces the intermixing.

This study furthers our understanding in oblique impact of two successive droplets on flat surfaces. In the near future, the effects of other parameters on this dynamic process

will be further studied and reported.

Acknowledgement

SA would like to acknowledge the financial support from The Hong Kong Polytechnic University for his PhD study. The authors also gratefully acknowledge the financial support for this study from The Research Grants Council of Hong Kong under General Research Fund (Project No.: PolyU 152493/16E) and the Departmental General Research Fund (G-UB51) from the Department of Mechanical Engineering of The Hong Kong Polytechnic University.

References

[1] R.E. Saunders, J.E. Gough, B. Derby, Delivery of human fibroblast cells by piezoelectric drop-on-demand inkjet printing, Biomaterials. 29 (2008) 193–203.

[2] D. Soltman, V. Subramanian, and V. Subramanian, Inkjet-Printed Line Morphologies and Temperature Control of the Coffee Ring Effect, Langmuir. 24 (2008) 2224–2231.

[3] W.M. Grissom, F.A. Wierum, Liquid spray cooling of a heated surface, Int. J. Heat Mass Transf. 24 (1981) 261–271.

[4] T.M. Squires, S.R. Quake, Microfluidics: Fluid physics at the nanoliter scale, Rev. Mod. Phys. 77 (2005) 977–1026.

[5] R. Rioboo, M. Marengo, C. Tropea, Time evolution of liquid drop impact onto solid, dry surfaces, Exp. Fluids. 33 (2002) 112–124.

[6] A. Asai, M. Shioya, S. Hirasawa, T. Okazaki, Impact of an ink drop on paper, J. Imaging Sci. Technol. 37 (1993) 205–207.

[7] A. Gupta, R. Kumar, Droplet impingement and breakup on a dry surface, Comput. Fluids. 39 (2010) 1696–1703.

[8] A. Gupta, R. Kumar, Two-dimensional lattice Boltzmann model for droplet impingement and breakup in low density ratio liquids, Commun. Comput. Phys. 10 (2011) 767–784.

[9] D. Zhang, K. Papadikis, S. Gu, Application of a high density ratio lattice-

Boltzmann model for the droplet impingement on flat and spherical surfaces, Int. J. Therm. Sci. 84 (2014) 75–85.

[10] M. Pasandideh-Fard, Y.M. Qiao, S. Chandra, J. Mostaghimi, Capillary effects during droplet impact on a solid surface, Phys. Fluids. 8 (1996) 650.

[11] T. Mao, D. Kuhn, H. Tran, Spread and rebound of liquid droplets upon impact on flat surfaces, AIChE J. 43 (1997) 2169–2179.

[12] S. Chandra, C. T. Avedisian, On the Collision of a Droplet with a Solid Surface, in: Proc. R. Soc. London A, 1991: p. 13.

[13] K.A. Raman, R.K. Jaiman, T. Lee, H. Low, A numerical study on electrowetting-induced jumping and transport of droplet, Int. J. Heat Mass Transf. 99 (2016) 805–821.

[14] A.L. Yarin, Drop impact dynamics: Splashing, Spreading, Receding, Bouncing…, Annu. Rev. Fluid Mech. 38 (2006) 159–192.

[15] Š. Šikalo, C. Tropea, E.N. Ganić, Impact of droplets onto inclined surfaces, J. Colloid Interface Sci. 286 (2005) 661–669.

[16] S.F. Lunkad, V. V. Buwa, K.D.P. Nigam, Numerical simulations of drop impact and spreading on horizontal and inclined surfaces, Chem. Eng. Sci. 62 (2007) 7214–7224.

[17] C. Shen, C. Yu, Y. Chen, Spreading dynamics of droplet on an inclined surface, Theor. Comput. Fluid Dyn. 30 (2016) 237–252.

[18] R. Li, N. Ashgriz, S. Chandra, J.R. Andrews, S. Drappel, Coalescence of two droplets impacting a solid surface, Exp. Fluids. 48 (2010) 1025–1035.

[19] P.J. Graham, M.M. Farhangi, A. Dolatabadi, Dynamics of droplet coalescence in response to increasing hydrophobicity, Phys. Fluids. 24 (2012).

[20] J.R. Castrejón-Pita, K.J. Kubiak, A.A. Castrejón-Pita, M.C.T. Wilson, I.M. Hutchings, Mixing and internal dynamics of droplets impacting and coalescing on a solid surface, Phys. Rev. E - Stat. Nonlinear, Soft Matter Phys. 88 (2013).

[21] I. V Roisman, B. Prunet-Foch, C. Tropea, M. Vignes-Adler, Multiple Drop Impact onto a Dry Solid Substrate, J. Colloid Interface Sci. 256 (2002) 396–410.

[22] K.A. Raman, R.K. Jaiman, T.S. Lee, H.T. Low, Computers & Fluids On the dynamics of crown structure in simultaneous two droplets impact onto stationary and moving liquid film, Comput. FLUIDS. 107 (2015) 285–300.

[23] J. Wu, J.J. Huang, W.W. Yan, Lattice Boltzmann investigation of droplets impact behaviors onto a solid substrate, Colloids Surfaces A Physicochem. Eng. Asp. 484

(2015) 318–328.

[24] W. Zhou, D. Loney, A.G. Fedorov, F.L. Degertekin, D.W. Rosen, Lattice Boltzmann simulations of multiple-droplet interaction dynamics, Phys. Rev. E. 89 (2014) 33311.

[25] H. Fujimoto, S. Ito, I. Takezaki, Experimental study of successive collision of two water droplets with a solid, Exp. Fluids. 33 (2002) 500–502.

[26] A.Y. Tong, S. Kasliwal, H. Fujimoto, On the Successive Impingement of Droplets Onto a Substrate, Numer. Heat Transf. Part A Appl. 52 (2007) 531–548.

[27] K. Ashoke Raman, R.K. Jaiman, T.S. Lee, H.T. Low, Lattice Boltzmann study on the dynamics of successive droplets impact on a solid surface, Chem. Eng. Sci. 145 (2016) 181–195.

[28] K. Ashoke Raman, R.K. Jaiman, T.-S. Lee, H.-T. Low, Dynamics of simultaneously impinging drops on a dry surface: Role of impact velocity and air inertia, J. Colloid Interface Sci. 486 (2017) 265–276.

[29] J.K. Domen, W.T. Stringfellow, M. Kay, C. Shelly, Fog water as an alternative and sustainable water resource, Clean Techn Env. Policy. 16 (2014) 235–249.

[30] K.-C. Park, S.S. Chhatre, S. Srinivasan, R.E. Cohen, G.H. McKinley, Optimal Design of Permeable Fiber Network Structures for Fog Harvesting, Langmuir. 29 (2013) 13269–13277.

[31] M. Massinon, H. Boukhalfa, F. Lebeau, The effect of surface orientation on spray retention, Precis. Agric. 15 (2014) 241–254.

[32] B. L. Scheller, D.W. Bousfield, Newtonian Drop Impact with a Solid Surface, AIChE Journal, 41(6). 41 (1995) 1357–1367.

[33] S. Chen, G.D. Doolen, Lattice Boltzmann Method for Fluid Flows, 30 (1998) 329–364.

[34] D. Raabe, Overview of the lattice Boltzmann method for nano- and microscale fluid dynamics in materials science and engineering, Model. Simul. Mater. Sci. Eng. 12 (2004) R13–R46.

[35] A. A. Mohammed, Lattice Boltzmann Method: Fundamentals and Engineering Applications with Computer Codes, 2012.

[36] R. Benzi, S. Succi, M. Vergassola, The lattice Boltzmann equation: theory and applications, Phys. Rep. 222 (1992) 145–197.

[37] X. He, S. Chen, R. Zhang, A Lattice Boltzmann Scheme for Incompressible Multiphase Flow and Its Application in Simulation of Rayleigh – Taylor Instability

1, J. Comput. Phys. 663 (1999) 642–663.

[38] R. Zhang, X. He, S. Chen, Interface and surface tension in incompressible lattice Boltzmann multiphase model, Comput. Phys. Commun. 129 (2000) 121–130.

[39] Š. Šikalo, H.D. Wilhelm, I. V. Roisman, S. Jakirlić, C. Tropea, Dynamic contact angle of spreading droplets: Experiments and simulations, Phys. Fluids. 17 (2005) 1–13.

[40] L. Wang, H. Huang, X.-Y. Lu, Scheme for contact angle and its hysteresis in a multiphase lattice Boltzmann method, Phys. Rev. E. 87 (2013) 13301.

[41] X. Gu, A. Gupta, R. Kumar, C.F. Blvd, Lattice Boltzmann Simulation of Drop Collision and Surface Impingement At High Density Ratio, AIAA (2009) 1–24.

[42] M. Taghilou, M.H. Rahimian, Lattice Boltzmann model for thermal behavior of a droplet on the solid surface, Int. J. Therm. Sci. 86 (2014) 1–11.